Z. Angew. Math. Phys. (2017) 68:82

0044-2275/17/040001-20
published online July 4, 2017
DOI 10.1007/s00033-017-0826-4

Zeitschrift für angewandte Mathematik und Physik ZAMP

Asymptotic approximations for pure bending of thin cylindrical shells

Ciprian D. Coman

Abstract. A simplified partial wrinkling scenario for in-plane bending of thin cylindrical shells is explored by using several asymptotic strategies. The eighth-order boundary eigenvalue problem investigated here originates in the Donnel–Mushtari–Vlasov shallow shell theory coupled with a linear membrane pre-bifurcation state. It is shown that the corresponding neutral stability curve is amenable to a detailed asymptotic analysis based on the method of multiple scales. This is further complemented by an alternative WKB approximation that provides comparable information with significantly less effort.

Mathematics Subject Classification. 74K25 thin shells, 34E20 asymptotics, WKB methods, singular perturbations, 74G60 bifurcation & buckling.

Keywords. Cylindrical shells, Wrinkling, Shallow shell equations, Multiple-scale asymptotics, WKB approximations.

1. Introduction

Thin-walled cylinders are used extensively in many industrial applications and are typically subjected to a variety of loadings, including axial, torsional and pressure loads; the main modes of failure in these cases have been reasonably well understood for some time (cf. [1]). However, the collapse of cylindrical shells under *in-plane* (or *pure*) *bending* is a significantly more complex situation that has, comparatively, attracted much less attention. By 'in-plane bending' here, we mean that systems of forces are applied on both ends of the cylinder such that they are each statically equivalent to a moment acting in the plane of curvature of the shell. It is beyond the scope of the present study to pursue a comprehensive review of the literature in this area, and we refer the interested reader to the excellent accounts given in [2,3]. To set the stage for the work included in the remainder of this paper, below we give a distilled historical outline relevant to our immediate purposes.

As early as 1927, Brazier [4] succeeded in determining the maximum bending moment carried by an infinitely long cylinder; he derived a nonlinear relation between the applied bending moment and the change of axial curvature by means of a simple-minded energy approach. Those results revealed that the cross section of the cylinder flattens progressively as the applied load increases, an effect which is intimately linked to the longitudinal tension and compression resisting the applied bending moment (see Fig. 1). Thus, the flexural stiffness of the deformed configuration is being reduced as the axial curvature increases and, consequently, the bending moment, which is specified as the product between curvature and flexural stiffness, reaches a maximum value. Brazier's analysis did not take into account explicitly the localised deformation present on the compressed side of the shell, a characteristic feature observed in many experiments [5–7] and which is indicative of a bifurcation-type instability.

Building upon earlier work by Flügge [8], Seide and Weingarten [9] were the first to carry out a numerical bifurcation analysis of the aforementioned problem by employing the Donnell–Mushtari–Vlasov (DMV) theory for shallow shells (e.g. [10,11]) in conjunction with a linear membrane pre-buckling state. The focus of their work was on short-length cylinders with simply supported ends. They found that

The original version of this article was revised: Due to a typesetting error, Eq. 5.9 was incorrect in the original publication and it has been corrected now.

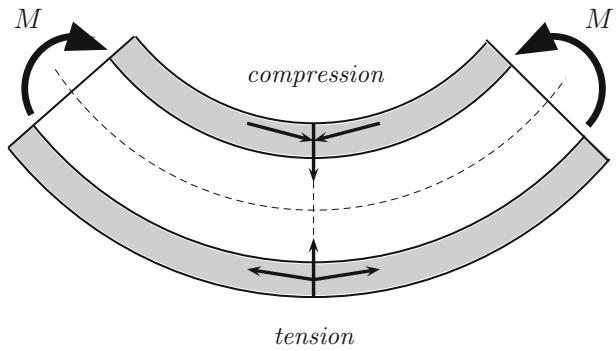

FIG. 1. A sketch of the axial cross section of a cylindrical shell showing the longitudinal tension and compression stresses due to the applied bending moment M. The thickness of the shell walls (the *grey areas*) is exaggerated for illustration purposes

the maximum axial stress at the bifurcation point is nearly equal to the classical buckling stress for a cylindrical shell subjected to uniform axial compression, and that the failure mode is characterised by small ripples confined to the compressed side of the shell. The bifurcation bending moment calculated in reference [9] is almost twice the value found by Brazier. This suggested that there are at least two distinct types of collapse modes corresponding to short and long cylinders, respectively.

According to Axelrad [12,13] the two collapse mechanisms can be unified by applying the *local buckling hypothesis* to a nonlinear pre-buckling deformation based upon a semi-membrane shell theory (e.g. see [3,14]). In its simplest form, the local buckling hypothesis assumes that the critical compression stress is equal to the buckling stress of a uniformly compressed cylinder, with the cylinder radius replaced by the actual local radius of curvature in the buckling zone of the shell. Using this local buckling approach, Axelrad concluded that the nonlinear pre-buckling deformation characterised by cross-sectional flattening is a dominant effect on the reduction of the critical bending moment. For very short cylinders, such ovalisation is prevented by the end conditions and the critical bending moment coincides with the result of Seide and Weingarten. On the other hand, for longer cylinders the flattening is more pronounced and the critical bending moment decreases, eventually approaching Brazier's collapse bending moment for infinitely long cylindrical shells. An idealised sketch of the moment–curvature diagram for a cylindrical shell of arbitrary length is included in Fig. 2.

Axelrad's work was later complemented by a more comprehensive investigation by Fabian [15], who explored the interaction of bifurcation and limit-point failure in long cylindrical tubes under pressure, axial compression and bending. A nonlinear pre-buckling solution was developed, based on an extension of Reissner's earlier work [14], and shallow shell theory was still adopted for the buckling and post-buckling regimes. However, Fabian's work did not clarify whether the bifurcation brings about collapse, but the numerical results he presented showed that without axial load, the bifurcation and the limit moments almost coincide. To examine the interaction between the bifurcation buckling and the limit failure of long cylinders, Stephens et al. [16] investigated numerically the case of a long isotropic circular cylinder under in-plane bending and defined a transition region between the classical buckling of short cylinders, on the one hand, and the Brazier collapse of very long cylinders, on the other. In this transition region, the circular cross section deforms into an oval shape after which the shell buckles into a short-wavelength pattern. Thus, the failure is due to the *interaction* of the two modes. They also confirmed the accuracy of Axelrad's earlier results [12] and pointed out the inherent difficulties associated with detecting the onset of the wrinkling deformations (originating in their very small amplitude relative to the other dimensions of the shell). In order to excite the bifurcation from the nonlinear pre-buckling state, a small initial imperfection with a short-wave axial mode was included in the analysis; the collapse due to bifurcation

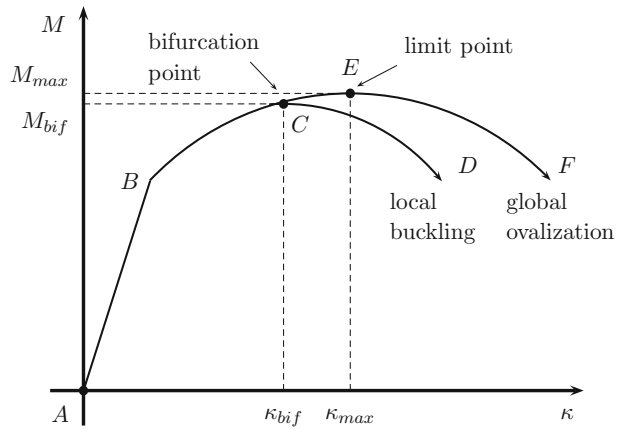

FIG. 2. Typical *moment* (M) versus (average) *axial curvature* (κ) diagram for a cylindrical shell subjected to pure bending. The deformation of short shells follows the path AB. Medium-length configurations experience in addition a certain amount of nonlinear behaviour (i.e. ovalisation of the cross section), and this corresponds to the path BC. Very long shells fail by a limit-point instability—the location of this event is marked as E. For completeness, we also record the sub-critical paths following the onset of the instability

was then assumed to be triggered when a relatively large growth of the imperfection occurred for a small increase in the bending moment. The same technical device was used in [6,17] for studying elasto-plastic bending of long tubes.

With this background in mind, the aims of this article are twofold. First, we show that the problem studied by Seide and Weingarten [9] is amenable to a fairly natural multiple-scale asymptotic analysis. Although this technique is prevalent in studies of nonlinear dynamics (e.g. [18]), its application to *linear* boundary-value problems in the literature seems to be scarce. Two notable exceptions that belong to the realm of fluid mechanics are those by Tam [19] and Long [20]; also, Wollkind [21] and Bouthier [22] have given comparisons of the main similarities and differences between the method of multiple scales and traditional matched asymptotics approaches. Second, we are motivated to extend the applicability of the asymptotic strategy originally proposed by Coman and Haughton in [23] for a class of wrinkling problems involving flat elastic plates subjected to in-plane loads (see also [24,25]). We show that this is indeed feasible, by first making some additional simplifications in the DMV system governing the bifurcations of our elastic tube. A slightly more general problem than that of [9], which includes variable mechanical/geometrical properties, was tackled by Tovstik and Smirnov [26] with the help of a Maslov-type WKB approximation. Their results are equivalent to those obtained in this paper by using the more elementary multiple-scale approach, but they are intrinsically linear. By contrast, the route taken here can be easily extended to cope with nonlinearities (e.g. post-buckling regime—see [27]).

The remainder of the paper is organised in the following way. We begin in the next section with a succinct review of the bifurcation equations from [9]; unlike in that reference, here the DMV system is kept in its standard form, without reducing it to a single eighth-order equation. The numerical investigations outlined in Sect. 3 suggest that the neutral stability curve for our system has a parabola-shaped appearance and is characterised by three distinct types of behaviour; these are associated with the global minimum, and the right and left branches, respectively. In Sect. 4 we deal with an asymptotic approximation for the energy-minimum configurations of the bent elastic cylinder, while Sects. 5 and 6 contain similar analyses for the other two regimes. A novel simplification of the bifurcation equations is also discussed briefly in Sect. 7, where we indicate how a traditional WKB strategy can lead to approximations comparable to those obtained in the earlier sections. The paper concludes with a discussion of our main findings.

2. The bifurcation equations

We consider a thin cylindrical shell of length L, radius R and uniform thickness h ($0 < h/R \ll 1$) subjected to compressive axial forces $P > 0$ and in-plane bending moments $M > 0$, as indicated in Fig. 3. To accomplish the loading in the axial direction, the cylinder is assumed to be bounded by light bulkheads or deep stiffeners, which are stiff in their own planes but may be readily warped out of their planes. The cylinder is also assumed to be made of an isotropic elastic material characterised by the Young's modulus $E > 0$ and the Poisson's ratio $0 < \nu < 1/2$.

The starting point for setting up the relevant bifurcation problem is the well-known Donnell–Mushtari–Vlasov (DMV) shallow shell buckling equations (e.g. see [10,11]) formulated in terms of the transverse displacement $w \equiv w(x,\theta)$ and a stress function $F \equiv F(x,\theta)$. If we let $\mathring{\sigma}_{xx}$, $\mathring{\sigma}_{x\theta}$ and $\mathring{\sigma}_{\theta\theta}$ be the distribution of pre-buckling membrane stresses in the cylinder, then the aforementioned equations can be expressed as

$$D\nabla^4 w - h\left(\mathring{\sigma}_{xx}\frac{\partial^2 w}{\partial x^2} + 2\mathring{\sigma}_{x\theta}\frac{1}{R}\frac{\partial^2 w}{\partial x\partial\theta} + \mathring{\sigma}_{\theta\theta}\frac{1}{R^2}\frac{\partial^2 w}{\partial\theta^2}\right) - \frac{h}{R}\left(\frac{\partial^2 F}{\partial x^2}\right) = 0, \tag{2.1a}$$

$$\nabla^4 F + \frac{E}{R}\left(\frac{\partial^2 w}{\partial x^2}\right) = 0, \tag{2.1b}$$

where $D \equiv Eh^3/12(1-\nu^2)$ represents the bending rigidity and the Laplacian is defined according to

$$\nabla^2 = \frac{\partial^2}{\partial x^2} + \frac{1}{R^2}\frac{\partial^2}{\partial\theta^2}.$$

Following Seide & Weingarten [9], prior to buckling the deformation of the cylindrical shell is taken to be described by a linear membrane state of stress. This leads to the well-known closed-form solution for the in-plane stresses (e.g. see [11])

$$\mathring{\sigma}_{xx} = -(\sigma_C + \sigma_B\cos\theta), \qquad \mathring{\sigma}_{x\theta} = \mathring{\sigma}_{\theta\theta} \equiv 0, \tag{2.2}$$

where

$$\sigma_C \equiv \frac{P}{2\pi Rh} \qquad \text{and} \qquad \sigma_B \equiv \frac{M}{\pi R^2 h}. \tag{2.3}$$

On substituting (2.2) and (2.3) into (2.1), the resulting equations can be simplified by looking for solutions with separable variables,

$$\begin{bmatrix} w(x,\theta) \\ F(x,\theta) \end{bmatrix} = \begin{bmatrix} G(\theta) \\ H(\theta) \end{bmatrix} \sin\left(\frac{\lambda_m x}{R}\right), \tag{2.4}$$

where

$$\lambda_m := \frac{m\pi R}{L}, \qquad (m = 1, 2, \dots) \tag{2.5}$$

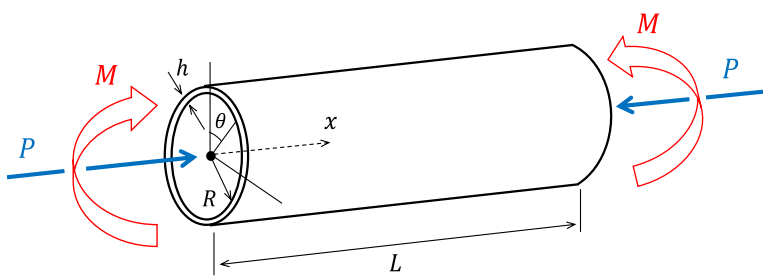

FIG. 3. Nomenclature for the cylindrical shell

represents the *axial* buckle half-wavelength, and the azimuthal amplitudes $H \equiv H(\theta)$, $G \equiv G(\theta)$ denote the new main dependent variables. Use of (2.4) in (2.1) results in a set of two coupled fourth-order ordinary differential equations for G and H, which are conveniently simplified further by introducing the dimensionless quantities

$$\overline{G} := \frac{G}{R}, \qquad \overline{H} := 12(1-\nu^2)\frac{H}{Eh^2}, \qquad \mu := \left[3(1-\nu^2)\right]^{1/2}\frac{R}{h}, \tag{2.6a}$$

$$K_C := \frac{\sigma_C}{\sigma_*}, \qquad K_B := \frac{\sigma_B}{\sigma_*}, \qquad \sigma_* := \frac{E}{[3(1-\nu^2)]^{1/2}}\left(\frac{h}{R}\right). \tag{2.6b}$$

We note in passing that σ_* represents the theoretical *compressive buckling stress* for long elastic cylindrical shells. Dropping the bars on the re-scaled variables, the reduced bifurcation equations can then be cast more compactly as

$$\begin{bmatrix} \mathcal{L}_{11} & \mathcal{L}_{12} \\ \mathcal{L}_{21} & \mathcal{L}_{22} \end{bmatrix} \begin{bmatrix} G(\theta) \\ H(\theta) \end{bmatrix} = \begin{bmatrix} 0 \\ 0 \end{bmatrix} \qquad \text{for} \quad -\pi \le \theta < \pi, \tag{2.7}$$

where we have introduced the differential operators

$$\mathcal{L}_{11} \equiv \frac{\mathrm{d}^4}{\mathrm{d}\theta^4} - 2\lambda_m^2\frac{\mathrm{d}^2}{\mathrm{d}\theta^2} + \lambda_m^2\left[\lambda_m^2 - 4\mu(K_C + K_B\cos\theta)\right], \quad \mathcal{L}_{12} \equiv \lambda_m^2, \tag{2.8a}$$

$$\mathcal{L}_{21} \equiv -4\lambda_m^2\mu^2, \quad \mathcal{L}_{22} \equiv \frac{\mathrm{d}^4}{\mathrm{d}\theta^4} - 2\lambda_m^2\frac{\mathrm{d}^2}{\mathrm{d}\theta^2} + \lambda_m^4. \tag{2.8b}$$

Given the nature of the main dependent variables in (2.7), appropriate periodicity conditions need to be imposed on $G \equiv G(\theta)$ and $H \equiv H(\theta)$. Using the symmetry properties of the equations it turns out that the eigenmodes can be either *even* (symmetric) or *odd* (anti-symmetric) functions. In the former case, $G(-\theta) = G(\theta)$ and $H(-\theta) = H(\theta)$ for all $\theta \in (-\pi, \pi]$, and thus the boundary conditions can be expressed as

$$G' = G''' = H' = H''' = 0, \qquad \text{for} \quad \theta \in \{0, \pi\}, \tag{2.9}$$

whereas for the odd modes, which satisfy $G(-\theta) = -G(\theta)$ and $H(-\theta) = -H(\theta)$ for all $\theta \in (-\pi, \pi]$, these boundary constraints must be changed to

$$G = G'' = H = H'' = 0, \qquad \text{for} \quad \theta \in \{0, \pi\}. \tag{2.10}$$

In the boundary-value problems consisting of Eq. (2.7) subject to either (2.9) or (2.10), the quantity $K_C \in \mathbb{R}$ is taken to be given, while $K_B = K_B(\lambda_m; \mu)$ represents the unknown eigenvalue. It is further noted that $\lambda_m > 0$ (or equivalently $m \in \mathbb{N}$) is also unknown at this stage and, for each fixed $\mu > 0$, this must be determined so that it renders the global minimum of the curve K_B vs. λ_m. The *critical* eigenvalue, $K_B^{(c)}$, and the *critical* buckle wavelength, λ_m^c, are thus defined by the requirements

$$K_B^{(c)} := \min_{\lambda_m > 0} K_B(\lambda_m; \mu), \qquad \text{with} \quad K_B^{(c)} = K_B(\lambda_m^c; \mu). \tag{2.11}$$

3. Numerical solutions

A limited set of numerical results for the boundary-value problems described in the previous section was originally reported by Seide & Weingarten [9]. Instead of (2.1) they relied on an equivalent form of the DMV equations that involves only the transverse displacement (this simplification is essentially due to Batdorf [28]), with the azimuthal amplitude $G(\theta)$ in (2.4) being resolved in a cosine Fourier series whose unknown coefficients were subsequently identified via a systematic Galerkin-type computational strategy. Our own numerical simulations of (2.7)-(2.9) have led to identical results as in [9]. In anticipation of the later asymptotic analyses, we take this opportunity to expand on the earlier numerical results so that we have a more rounded picture of the expected behaviour of the eigenmodes. For brevity, the main focus

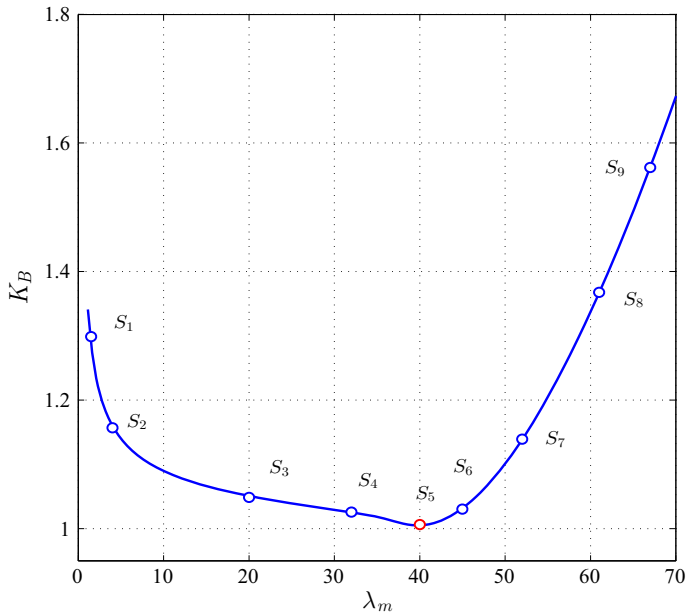

FIG. 4. A typical *neutral stability curve* for the pure bending problem (i.e. $K_C \equiv 0$) corresponding to $R/h = 500$ and $\nu = 0.3$. The round markers, labelled S_j $(j = 1, 2, \ldots, 9)$, indicate sequences of points on either side of the absolute minimum of this curve (S_5)

will be on the case $K_C = 0$; if $K_C \neq 0$ there are some obvious quantitative changes in the results reported below, but the qualitative behaviour of the problem remains unaltered.

Although two different types of eigenmodes have been identified in the previous section, direct numerical simulations show that the even modes have lower energy, so we need not be concerned with the anti-symmetric ones. Included in Fig. 4 is a typical neutral stability curve, $\mathcal{C}$ (say), of the eigenproblem (2.7)–(2.9) for $R/h = 500$; we remark that $K_B \to \infty$ as either $\lambda_m \to 0^+$ or $\lambda_m \to +\infty$. To illustrate the changes undergone by the eigenmodes along the neutral stability curve, a number of arbitrary points S_j $(j = 1, 2, \ldots, 9)$ have been selected on either side of the unique global minimum point marked as S_5 (the abscissa of this point coincides with λ_m^c, while the vertical coordinate represents $K_B^{(c)}$). For convenience we shall write $\mathcal{C} = \mathcal{C}^{(-)} \cup \mathcal{C}^{(+)}$, where $\mathcal{C}^{(+)} \equiv \{(\lambda_m, K_B) \in \mathbb{R}^2 \mid \lambda_m \geq \lambda_m^c\}$ and $\mathcal{C}^{(-)} \equiv \{(\lambda_m, K_B) \in \mathbb{R}^2 \mid \lambda_m \leq \lambda_m^c\}$.

The solutions corresponding to the left branch $\mathcal{C}^{(-)}$ (i.e. S_j with $j = 1, 2, \ldots, 5$) are plotted in Fig. 5; for $0 < \lambda_m \ll \lambda_m^c$, these functions take the form of a spatial fast oscillation modulated over a slower spatial scale, but as λ_m grows the frequency of the fast oscillation decreases and its envelope steepens. In the limit $\lambda_m \to \lambda_m^{c+}$ it turns out that the eigenmodes have a much simpler spatial structure in the form of a 'bump' localised near $\theta = 0$. Interestingly, on $\mathcal{C}^{(+)}$ the corresponding solutions (e.g. S_j with $j = 6, 7, 8, 9$) remain (almost) similar to the critical mode (S_5), experiencing a slight growth in the transverse direction as λ_m moves away from λ_m^c—see Fig. 6. It is perhaps worth emphasising that the modes $H(\theta)$ on both branches share the same properties as the ones recorded in the aforementioned figures, and for this reason they are left out.

From a practical point of view, the eigenmodes associated with the minima of the neutral stability curves are the most important ones, as they correspond to energy-minimum configurations of the partially wrinkled shell. The dependence of these functions on the (dimensionless) thickness parameter R/h is investigated in Fig. 7. Displayed in the left window are a set of neutral stability curves for values $10^2 \leq R/h \leq 15 \times 10^2$; their minima are indicated by the round (red) markers, while the right window contains

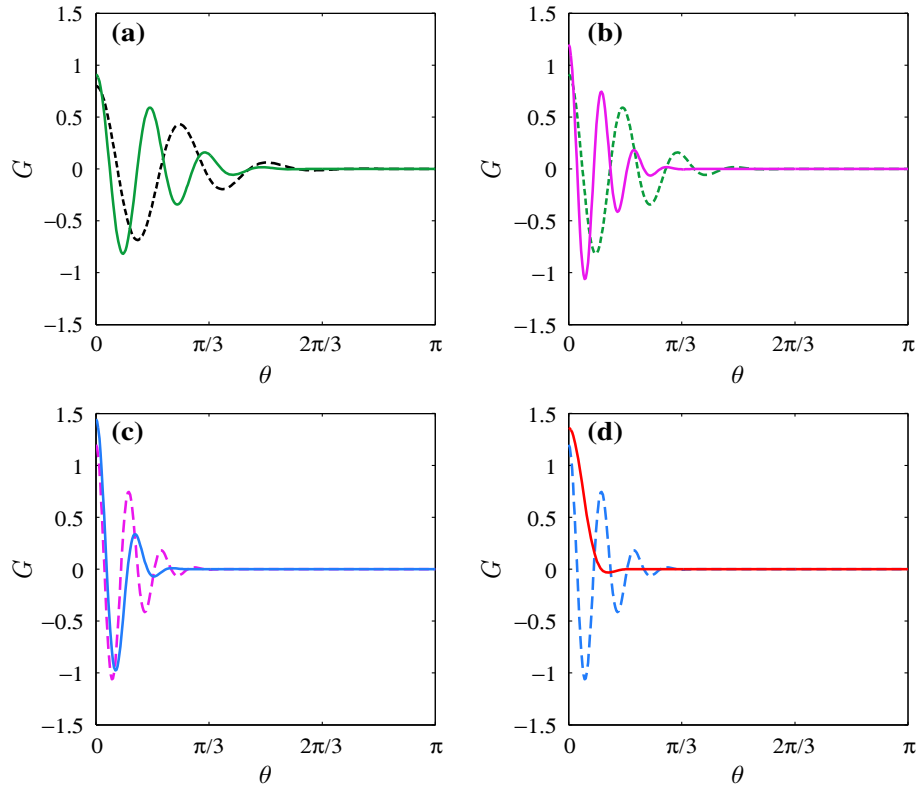

FIG. 5. Morphology of the localised eigenmodes along the *left branch* of the curve shown in Fig. 4. Each window contains the pair (S_j, S_{j+1}) corresponding to: **a** $j = 1$, **b** $j = 2$, **c** $j = 3$, **d** $j = 4$; S_j is indicated by the *dash line*, while S_{j+1} represents the continuous curve

the corresponding critical eigenmodes. It is clear that as the thickness decreases there is another form of localisation that affects these critical modes. Furthermore, there is strong evidence in the left window suggesting that $\lim_{\mu\to\infty} K_B^{(c)} = 1$ and $\lim_{\mu\to\infty} \lambda_m^c \gg 1$.

Due to the particular definition of the axial wavelength (2.5), the information in Fig. 4 can be presented in a more informative way that takes explicitly into account that L and R are given quantities, whereas $m \in \mathbb{N}$ is variable and has to be found as part of the solution. This information appears in Fig. 8, where on the horizontal axis we record $L/\pi R \equiv m/\lambda_m$; in the left window the curves correspond to $m = 1, 2, \ldots, 10$, while on the right we have $m = 33, 34, \ldots, 61$. The red solid section of each such curve delineates the range of values $L/\pi R$ for which the corresponding $m \in \mathbb{N}$ leads to a critical λ_m^c, and the union of all these red sections forms the so-called *neutral stability envelope*. It should be clear that the data included in the left window of Fig. 8 concern cylinders that are very short and for which the analysis in this paper is not applicable. It is included here solely for contrast with the curves shown in the right window. We also note that for realistic $L/\pi R$ ratios the neutral stability envelope is almost flat and the critical m tends to be large.

4. The critical case

In this section, our goal is to find an asymptotic approximation for $K_B^{(c)}$ and λ_m^c defined in (2.11). This is facilitated by tentatively introducing two spatial scales

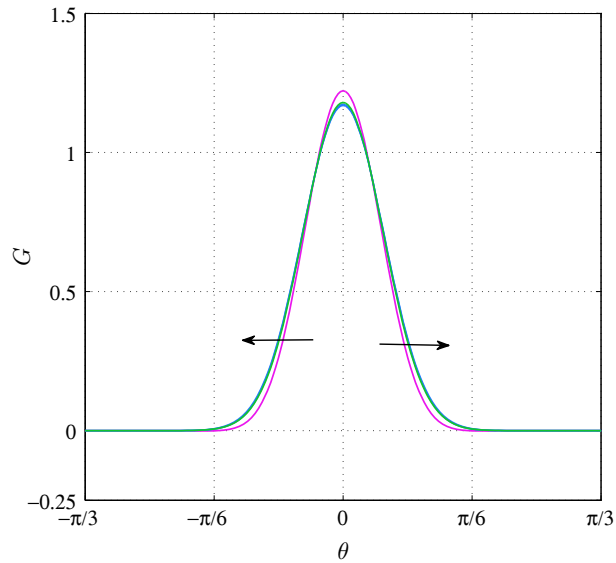

FIG. 6. Sequence of eigenmodes on $\mathcal{C}^{(+)}$ corresponding to the points S_j $(j = 6, 7, 8, 9)$ in Fig. 4; the arrows show the direction in which $|\lambda_m - \lambda_m^c|$ increases and the horizontal range has been restricted to $[-\pi/3, \pi/3]$ for the sake of clarity

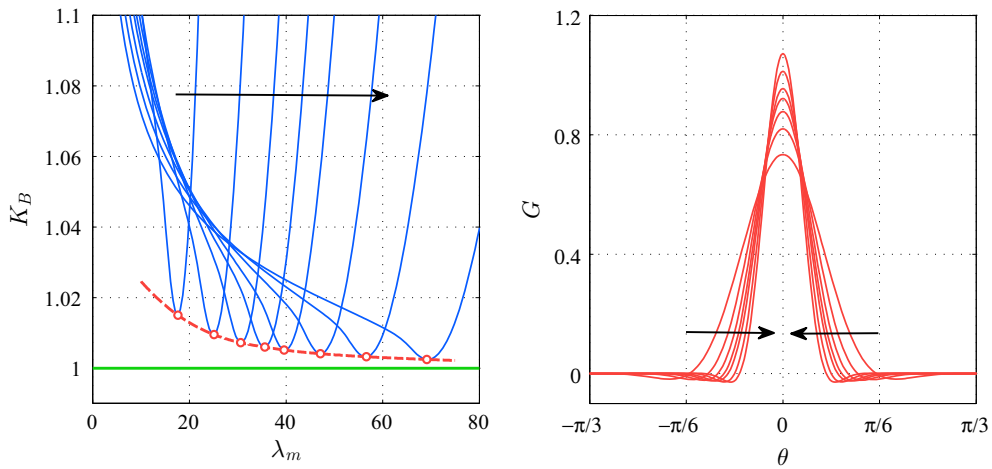

FIG. 7. Left: sample of neutral stability curves for the boundary-value problem (2.7)–(2.9) corresponding to $R/h = j \times 10^2$ $(j = 1, 2, 3, 4, 5, 7, 10, 15)$ and $K_C \equiv 0$; the arrow shows the direction in which this quantity increases. The round markers identify the absolute minima of these curves, and their locus is represented by the dashed curve. The localisation of the critical modes $(G \equiv G(\theta))$ associated with the round markers is illustrated in the right window; in the interest of clarity, the horizontal range has been restricted to $[-\pi/3, \pi/3]$ and the direction of the arrows has the same connotation as on the left

$$X_1 \equiv \mu^{1/2}\theta, \qquad X_2 \equiv \mu^{1/3}\theta,$$

and noting that the derivatives with respect to θ are transformed according to

$$\frac{\mathrm{d}}{\mathrm{d}\theta} = \mu^{1/2} D_1 + \mu^{1/3} D_2, \qquad D_j \equiv \frac{\partial}{\partial X_j} \qquad (j = 1, 2), \tag{4.1}$$

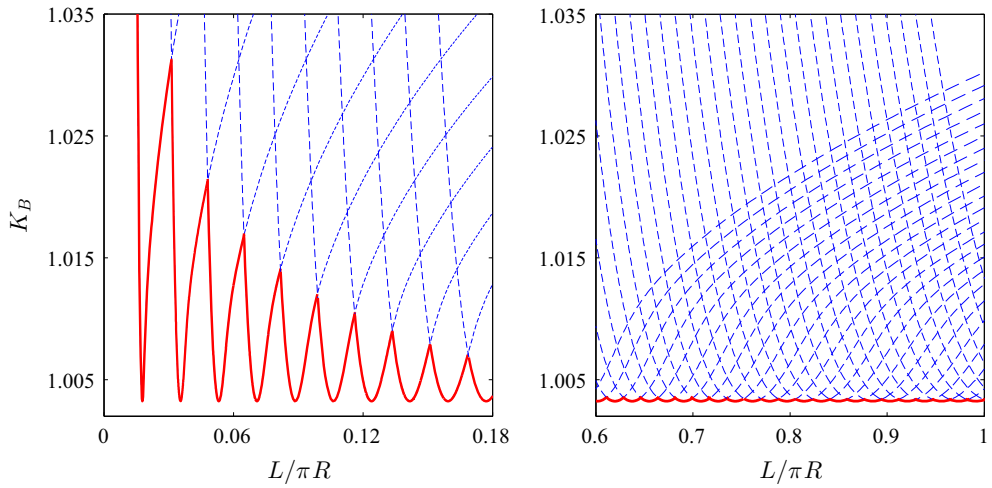

FIG. 8. Dependence of K_B on the (non-dimensional) length of the cylinder for $K_C \equiv 0$ and $R/h = 10^3$

generalised appropriately to higher-order derivatives. We look for a solution of (2.7) with an ansatz of the form

$$K_B = K_0 + K_1\mu^{-2/3} + \cdots, \tag{4.2a}$$

$$\lambda_m^2 = \eta_0\mu + \eta_1\mu^{2/3} + \eta_2\mu^{1/3} + \cdots, \tag{4.2b}$$

and

$$\boldsymbol{u} = \boldsymbol{u}^{(0)}(X_1, X_2) + \mu^{-1/3}\boldsymbol{u}^{(1)}(X_1, X_2) + \mu^{-2/3}\boldsymbol{u}^{(2)}(X_1, X_2) + \ldots, \tag{4.3}$$

where

$$\boldsymbol{u} := \begin{bmatrix} G \\ \mu^{-1}H \end{bmatrix}, \qquad \boldsymbol{u}^{(j)} := \begin{bmatrix} G_j \\ H_j \end{bmatrix}, \qquad (j = 0, 1, 2, \ldots).$$

Substituting (4.2) and (4.3) in the bifurcation system (2.7), we get at leading order

$$\begin{bmatrix} (D_1^2 - \eta_0)^2 - 4\eta_0 K_0 & \eta_0 \\ -4\eta_0 & (D_1^2 - \eta_0)^2 \end{bmatrix} \begin{bmatrix} G_0 \\ H_0 \end{bmatrix} = \begin{bmatrix} 0 \\ 0 \end{bmatrix}. \tag{4.4}$$

Since this is a constant-coefficient system, we look for solutions in the form $G_0 = \widehat{G}_0 \exp(pX_1)$ and $H_0 = \widehat{H}_0 \exp(pX_1)$, where p, $\widehat{G}_0$ and $\widehat{H}_0$ are yet to be found. The characteristic equation satisfied by p can be rearranged to give an expression for $K_0 = K_0(\eta_0; p)$, namely

$$K_0 = \frac{1}{4\eta_0}\left[(p^2 - \eta_0)^2 + \frac{4\eta_0^2}{(p^2 - \eta_0)^2}\right]. \tag{4.5}$$

Minimising (4.5) with respect to η_0 (i.e. solving $dK_0/d\eta_0 = 0$), we find

$$(p^2 - \eta_0)^4 = 4\eta_0^2. \tag{4.6}$$

This is just an eight-order algebraic equation in p which has the following roots

$$p_{\alpha\beta} = (-1)^\alpha[\eta_0 + (-1)^{\beta/2}\sqrt{2\eta_0}]^{1/2}, \qquad (\alpha = 1, 2;\ \beta = 1, \ldots, 4). \tag{4.7}$$

If $\eta_0 > 2$, none of the solutions associated with these characteristic roots will lead to a spatial (purely) harmonic behaviour. However, for $\eta_0 < 2$ the roots $p_{\alpha 2}$ $(\alpha = 1, 2)$ do meet this requirement, and we define

$$\omega_0 := (\sqrt{2\eta_0} - \eta_0)^{1/2}, \qquad \text{so that} \qquad p_{\alpha 2} = (-1)^\alpha \mathrm{i}\omega_0, \qquad (\alpha = 1, 2),$$

where $\mathrm{i} \equiv \sqrt{-1} \in \mathbb{C}$ is the usual imaginary unit. Since the critical eigenmodes do not contain a fast oscillatory component, we can set $\omega_0 = 0$, whereby $\eta_0 = 2$; in conjunction with (4.5) this then leads to $K_0 = 1$. Having suppressed the dependence on X_1, it remains that $G_j = G_j(X_2)$, $H_j = H_j(X_2)$ for $j = 0, 1, \ldots$ and our main task for the remaining of this section will be to find the leading-order terms G_0 and H_0, as well as K_1 and η_1 in (4.2).

We start by observing that in the differential operator that appears in (4.4) the derivative plays no role now, and it is thus reduced to an ordinary matrix, $\boldsymbol{M}$ (say). Using the ansatz (4.2) and (4.3) as indicated above, the first non-trivial equation we obtain can be expressed as

$$\boldsymbol{M}\boldsymbol{u}^{(1)} = \boldsymbol{f}^{(1)} := [\mathcal{R}_{11}, \mathcal{R}_{12}]^T, \tag{4.8}$$

$$\mathcal{R}_{11} := 2\eta_0 D_2^2 G_0 - \eta_1 H_0, \qquad \mathcal{R}_{12} := 4\eta_1 G_0 + 2\eta_0 D_2^2 H_0 - 2\eta_0\eta_1 H_0.$$

A close look at the system (4.8) indicates that it is equivalent to

$$-4G_1 + 2H_1 = 4D_2^2 G_0 - \eta_1 H_0. \tag{4.9}$$

The next non-trivial equations that we get from (2.7) are

$$\boldsymbol{M}\boldsymbol{u}^{(2)} = \boldsymbol{f}^{(2)} := [\mathcal{R}_{21}, \mathcal{R}_{22}]^T, \tag{4.10}$$

$$\mathcal{R}_{21} := -D_2^4 G_0 + 2\eta_0 D_2^2 G_1 + 2\eta_1 D_2^2 G_0 - \left[\eta_1^2 - 4\eta_0 K_1 + 2\eta_0 K_0 X_2^2\right] G_0 - \eta_1 H_1 - \eta_2 H_0,$$
$$\mathcal{R}_{22} := 4\eta_1 G_1 + 4\eta_2 G_0 - D_2^4 H_0 + 2\eta_0 D_2^2 H_1 + 2\eta_1 D_2^2 H_0 - 2\eta_0\eta_1 H_1 - (\eta_1^2 + 2\eta_0\eta_2) H_0.$$

Multiplying the first equation in (4.10) by 2 and subtracting the result from the second equation, followed by repeated use of (4.4) and (4.9), eventually lead to

$$\frac{\mathrm{d}^4 G_0}{\mathrm{d}X_2^4} - \eta_1 \frac{\mathrm{d}^2 G_0}{\mathrm{d}X_2^2} + \left(\frac{\eta_1^2 - 8K_1}{4} + X_2^2\right) G_0 = 0. \tag{4.11}$$

This must be solved subject to the boundary conditions

$$\frac{\mathrm{d}G_0}{\mathrm{d}X_2} = \frac{\mathrm{d}^3 G_0}{\mathrm{d}X_2^3} = 0, \qquad \text{for} \qquad X_2 = 0, \tag{4.12}$$

$$G_0 \to 0 \quad \text{and} \quad \frac{\mathrm{d}G_0}{\mathrm{d}X_2} \to 0, \qquad \text{as} \qquad X_2 \to +\infty. \tag{4.13}$$

We note that Eq. (4.11) together with the constraints (4.12) constitute an eigenvalue problem in which the eigenparameter K_1 depends on $\eta_1 \in \mathbb{R}$. As in this section we are ultimately interested in the *critical* wrinkling load, our aim is to minimise the function $K_1 = K_1(\eta_1)$. A standard numerical solution allows us to identify the value $\eta_1 = \eta_1^*$ for which the eigenvalue K_1 is least, K_1^* (say). In particular, we find $\eta_1^* \simeq -0.875$ and $K_1^* \simeq 0.45226$, so our approximation for the critical point of the neutral stability curve becomes

$$K_B = 1 + 0.45226\mu^{-2/3} + \cdots \qquad \text{and} \qquad \lambda_m = 1.4142\mu^{1/2} - 0.3094\mu^{1/6} + \cdots. \tag{4.14}$$

These formulae produce approximations that are within less than 1% of the original values computed by numerically integrating the ('even') boundary-value problem of Sect. 2.

Recalling definitions (2.6), it follows from (4.14) that $\sigma \to \sigma_*$ as $h \to 0$. Since the work [9] was entirely numerical, the conclusion reached by Seide and Weingarten was that the critical maximum membrane compressive stress was only slightly greater than that of the axially loaded shell. Libai and Durban [29] adopted the displacement form of the DMV equations with the basic state (2.2) in which $K_C = 0$, and made use of an ingenious series solution that allowed them to show that the two values actually coincide in the limit $h \to 0$.

5. The right branch

Routine scaling arguments suggest that for $\mu \gg 1$ the solutions of (2.7) situated on $\mathcal{C}^{(+)}$ are confined within a layer of thickness $\mathcal{O}(\mu^{-1/4})$ centred at $\theta = 0$. Thus, we are led to introduce the new re-scaled coordinate

$$Z = \mu^{1/4}\theta, \qquad Z = \mathcal{O}(1),$$

and set $\lambda_m^2 = \eta\mu$ for some $\eta = \mathcal{O}(1)$. Since we are exclusively interested in the right-hand branch of the neutral stability curve, it is clear that $\eta > 2$.

We look for a solution of (2.7) with an ansatz of the form

$$K_B = K_0 + K_1\mu^{-1/2} + K_2\mu^{-1} + \dots, \tag{5.1}$$

and

$$\boldsymbol{u} = \boldsymbol{u}^{(0)}(Z) + \mu^{-1/2}\boldsymbol{u}^{(1)}(Z) + \mu^{-1}\boldsymbol{u}^{(2)}(Z) + \dots, \tag{5.2}$$

where

$$\boldsymbol{u} := \begin{bmatrix} G \\ \mu^{-1}H \end{bmatrix}, \qquad \boldsymbol{u}^{(j)} := \begin{bmatrix} G_j \\ H_j \end{bmatrix}, \qquad (j = 0, 1, 2, \dots).$$

The constants $K_j = \mathcal{O}(1)$ in (5.1) and the individual terms $\boldsymbol{u}^{(j)}$ on the right-hand side of (5.2) are found as usual by substituting the assumed solution in the differential equations, collecting like powers of μ, and setting to zero the corresponding coefficients. The outcome is a hierarchy of equations that can be cast as

$$\boldsymbol{A}\boldsymbol{u}^{(j)} = \boldsymbol{b}^{(j)}, \qquad (j = 0, 1, 2, \dots), \tag{5.3}$$

with

$$\boldsymbol{A} := \begin{bmatrix} \eta(\eta - 4K_0) & \eta \\ -4\eta & \eta^2 \end{bmatrix}, \qquad \boldsymbol{b}^{(j)} := \begin{bmatrix} \mathcal{R}_{j1} \\ \mathcal{R}_{j2} \end{bmatrix},$$

and the components of the vectors $\boldsymbol{b}^{(j)}$ will be recorded below as we go along.

For the zeroth-order equations, we find $\mathcal{R}_{01} = \mathcal{R}_{02} \equiv 0$, so that we have a homogeneous system. This is consistent only if the determinant of the coefficient matrix is zero, that is

$$K_0 = \frac{1}{4}\left(\eta + \frac{4}{\eta}\right). \tag{5.4}$$

Clearly, $K_0 > 1$ for all $\eta \in (2, \infty)$, which reassures us that the leading-order approximation predicts the expected behaviour consistent with the regime we are presently investigating. Next, the right-hand side for the first-order equations corresponds to the components

$$\mathcal{R}_{11} := 2\eta\frac{\mathrm{d}^2G_0}{\mathrm{d}Z^2} + 4\eta K_1 G_0 - 2\eta K_0 Z^2 G_0, \qquad \mathcal{R}_{12} := 2\eta\frac{\mathrm{d}^2H_0}{\mathrm{d}Z^2}. \tag{5.5}$$

Since for $j = 1$ Eq. (5.3) represents an inhomogeneous system, its solvability demands that the right-hand side, $\boldsymbol{b}^{(1)}$, is orthogonal on the null space of the adjoint system. The solution of the adjoint equations is $\bar{\boldsymbol{u}} = \big[-1,\, 1/\eta\big]^T$, so the solvability requirement turns out to lead to

$$\frac{\mathrm{d}^2G_0}{\mathrm{d}Z^2} + (\gamma_1 - \gamma_2 Z^2)G_0 = 0, \tag{5.6}$$

where

$$\gamma_1 := \frac{2\eta^2 K_1}{\eta^2 - 4} \qquad \text{and} \qquad \gamma_2 := \frac{\eta^2 K_0}{\eta^2 - 4}.$$

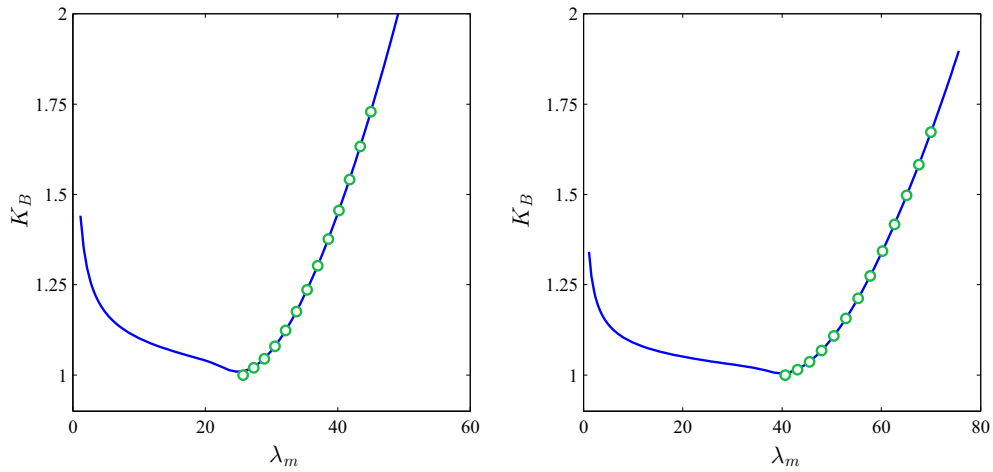

FIG. 9. Comparisons between the asymptotic predictions (5.9) (discrete markers) and direct numerical simulations of the original bifurcation problem (2.7)–(2.9) (continuous line) for $\nu = 0.3$; $R/h = 200$ (*left*) and $R/h = 500$ (*right*)

If we further ask for $G_0(Z) \to 0$ as $Z \to \pm\infty$, then we can extract K_1 from the resulting eigenvalue problem. We recall that the Weber–Hermite eigenvalue problem,

$$\begin{cases} W'' + \left(q + \dfrac{1}{2} - \dfrac{\zeta^2}{4}\right) W = 0, & -\infty < \zeta < \infty, \qquad (5.7a) \\ W(\zeta) \to 0 \quad \text{as} \quad \zeta \to \pm\infty, \qquad (5.7b) \end{cases}$$

admits non-trivial solutions only if q is a non-negative integer $q = 0, 1, 2, \ldots$ (e.g. see [30]). By changing the independent variable in (5.6) according to $Z =: (4\gamma_2)^{-1/4}\,\overline{Z}$, then $G_0 \equiv G_0(\overline{Z})$ satisfies a Weber–Hermite-type differential equation. Thus, in light of the remarks made above, we immediately deduce that $\gamma_1/\sqrt{\gamma_2} = 2i + 1$ for $i = 0, 1, 2, \ldots$; the lowest eigenvalue K_1 corresponds to $i = 0$. Putting together this result and (5.4), we then get

$$K_B = \frac{\eta^2 + 4}{4\eta} + \frac{(\eta^4 - 16)^{1/2}}{4\eta^{3/2}}\mu^{-1/2} + \ldots, \qquad (5.8)$$

or, after eliminating $\eta = \lambda_m^2 \mu^{-1}$,

$$K_B = \frac{1}{4\mu}\left(\lambda_m^2 + \frac{4\mu^2}{\lambda_m^2}\right)^{1/2}\left[\left(\lambda_m^2 + \frac{4\mu^2}{\lambda_m^2}\right)^{1/2} + \frac{1}{\lambda_m}\left(\lambda_m^2 - \frac{4\mu^2}{\lambda_m^2}\right)^{1/2}\right] + \ldots. \qquad (5.9)$$

Formula (5.9) represents an approximation for $\mathcal{C}^{(+)}$ valid for $\mu \gg 1$ and $\lambda_m > \lambda_m^c$. For the sake of completeness, in Fig. 9 we illustrate a sample of comparisons between this asymptotic result and direct numerical simulations of (2.7)–(2.9).

6. The left branch

The numerical solutions included in Sect. 3 suggested that on the left-hand branch of the neutral stability curve, $\mathcal{C}^{(-)}$, the solutions of (2.7) consist of a harmonic spatial oscillation modulated over a slower scale. This behaviour is very similar to that encountered in the related problem of a linear beam on an inhomogeneous Winkler foundation [27] (see also [31]). One of the main differences lies in the fact that here we have to deal with a system of two simultaneous equations.

Let us start by defining the re-scaled coordinates

$$X_1 \equiv \mu^{1/2}\theta, \qquad X_2 \equiv \mu^{1/4}\theta,$$

and note that the derivatives with respect to θ are now transformed according to

$$\frac{\mathrm{d}}{\mathrm{d}\theta} = \mu^{1/2}D_1 + \mu^{1/4}D_2, \qquad D_j \equiv \frac{\partial}{\partial X_j} \qquad (j = 1, 2), \tag{6.1}$$

generalised appropriately to higher-order derivatives. We shall look for a solution of (2.7) with an ansatz of the form

$$K_B = \sum_{j=0}^{\infty} K_j \mu^{-j/2} \qquad \text{and} \qquad \boldsymbol{u} = \sum_{j=0}^{\infty} \mu^{-j/4}\boldsymbol{u}^{(j)}(X_1, X_2), \tag{6.2}$$

where

$$\boldsymbol{u} := \begin{bmatrix} G \\ \mu^{-1}H \end{bmatrix}, \qquad \boldsymbol{u}^{(j)} := \begin{bmatrix} G_j \\ H_j \end{bmatrix}, \qquad (j = 0, 1, 2, \dots);$$

the constants $K_j = \mathcal{O}(1)$ and the individual terms $\boldsymbol{u}^{(j)}$ on the right-hand side of (6.2) are found as already explained in Sect. 5, by making the appropriate substitutions. This time the outcome is two hierarchies of equations that can be cast succinctly as

$$\boldsymbol{L}\boldsymbol{u}^{(j)} = \boldsymbol{f}^{(j)}, \qquad \text{for} \quad j = 0, 1, 2, \dots, \tag{6.3}$$

where $\boldsymbol{L}$ denotes the (matrix) differential operator that appears in (4.4) in which $\eta_0 \to \eta$ and $\boldsymbol{f}^{(j)} := [\mathcal{R}_{j1}, \mathcal{R}_{j2}]^T$; the components of this column vector will be recorded as we go along.

Note that we have already dealt with the zeroth-order problem, which corresponds to $\boldsymbol{f}^{(0)} \equiv \boldsymbol{0}$. Its solution is given by

$$G_0 = A(X_2)\cos(\omega_0 X_1), \qquad H_0 = 2G_0, \tag{6.4}$$

where the amplitude $A = A(X_2)$ will be fixed at higher orders; without loss of generality, we have set the phase angle to zero.

For the first-order problem, it transpires that

$$\mathcal{R}_{11} := -4D_1^3 D_2 G_0 + 4\eta D_1 D_2 G_0 \qquad \text{and} \qquad \mathcal{R}_{12} := -4D_1^3 D_2 H_0 + 4\eta D_1 D_2 H_0,$$

and the solution has the form

$$G_1 = B(X_2)\sin(\omega_0 X_1), \qquad H_1 = 2G_1 - 4\sqrt{2}\omega_0\eta^{-1/2}A'(X_2)\sin(\omega_0 X_1), \tag{6.5}$$

where the 'dash' denotes differentiation with respect to X_2.

Proceeding to the next order, routine calculations allow us to identify

$$\mathcal{R}_{21} := -4D_1^3 D_2 G_1 - 6D_1^2 D_2^2 G_0 + 4\eta D_1 D_2 G_1 + 2\eta D_2^2 G_0 + 4\eta K_1 G_0 - 2\eta K_0 X_2^2 G_0,$$
$$\mathcal{R}_{22} := -4D_1^3 D_2 H_1 - 6D_1^2 D_2^2 H_0 + 4\eta D_1 D_2 H_1 + 2\eta D_2^2 H_0.$$

Before we can find G_2 and H_2, the consistency condition needs to be imposed on the second-order system (6.3) (with $j = 2$). To this end, we multiply the first equation in the aforementioned system by 2 and subtract the result from the second one. Using (6.4) and (6.5), the resulting expressions can be simplified to yield

$$\mathcal{L}^{\#}[A] \equiv 8\omega_0^2 A'' + \eta(2K_1 - X_2^2)A = 0, \tag{6.6}$$

which is easily recognised as being just a re-scaled version of the Weber–Hermite equation already encountered in the previous section. Letting $X_2 =: 2^{1/4}\omega_0^{1/2}\eta^{-1/4}\overline{X}_2$ Eq. (6.6) changes into the standard form (5.7a), whereby we deduce that

$$K_1 = \sqrt{2}\,\omega_0\eta^{-1/2}. \tag{6.7}$$

The two-term asymptotic approximation obtained so far is accurate relatively far from the critical point $(\lambda_m^c, K_B^{(c)})$, but in its close proximity it overestimates the numerical result because $K_1 \to 0^+$ as $\lambda_m \to$

$\lambda_m^{c\,+}$, so the expansion (6.2a) loses its asymptotic character. Of course, within that range the critical regime approximation of Sect. 4 becomes relevant, so this is not a serious shortcoming. However, it turns out that this issue can be fixed, at least partially, by calculating the next-order term K_2 in (6.2a). Since the corresponding calculations are quite lengthy (but otherwise elementary), only a brief outline is given next.

The right-hand side of (6.3) for the third-order problem has components given by

$$\begin{aligned}\mathcal{R}_{31} := &-4D_1D_2^3G_0 - 6D_1^2D_2^2G_1 - 4D_1^3D_2G_2 + 2\eta D_2^2G_1\\ &+ 4\eta D_1D_2G_2 + 4\eta K_1G_1 - 2\eta X^2G_1,\end{aligned} \tag{6.8}$$

and

$$\mathcal{R}_{32} := -4D_1D_2^3H_0 - 6D_1^2D_2^2H_1 - 4D_1^3D_2H_2 + 2\eta D_2^2H_1 + 4\eta D_1D_2H_2.$$

Enforcing the consistency of the corresponding system as before yields the inhomogeneous Weber–Hermite equation

$$\mathcal{L}^{\#}[B] = -4\sqrt{2}\omega_0\left(2\eta^{1/2} - \sqrt{2}\right)A'''. \tag{6.9}$$

A particular solution of (6.9) is

$$B(X_2) = -\frac{1}{3}(2\eta - \sqrt{2\eta})\left[\left(\frac{\eta^{1/2}}{2\sqrt{2}\omega_0}\right)X^3 - 6X\right]A(X_2), \tag{6.10}$$

which then fixes the first-order terms (6.5).

The coefficient K_2 will be found from the next-order problem as it appears in the expression of the right-hand side $\boldsymbol{f}^{(4)}$, namely

$$\begin{aligned}\mathcal{R}_{41} := &-D_2^4G_0 - 4D_1D_2^3G_1 - 6D_1^2D_2^2G_2 - 4D_1^3D_2G_3 + 2\eta D_2^2G_2 + 4\eta D_1D_2G_3\\ &+ 4\eta K_1G_2 + \underline{4\eta K_2G_0} - 2\eta X^2G_2 - 2\eta K_1X^2G_0 + \frac{1}{6}\eta X^4G_0,\end{aligned} \tag{6.11}$$

and

$$\mathcal{R}_{42} := -D_2^4H_0 - 4D_1D_2^3H_1 - 6D_1^2D_2^2H_2 - 4D_1^3D_2H_3 + 2\eta D_2^2H_2 + 4\eta D_1D_2H_3.$$

In enforcing the consistency of the equations at this order (as was done before), we need the solution of the earlier second-order problem that contains a degree of arbitrariness, in the sense that $G_2 = C(X_2)\cos(\omega_0X_1)$, and the function $C \equiv C(X_2)$ is unknown at that stage. The result of the consistency condition can be shown to take the form of the second-order inhomogeneous Weber–Hermite equation

$$\mathcal{L}^{\#}[C] = d_{13}B''' + d_{04}A'''' + d_{00}A - 2\eta K_2A, \tag{6.12}$$

with

$$d_{13} \equiv 8\omega_0(\sqrt{2}\eta^{1/2} - 1), \qquad d_{04} \equiv 18 - 46\sqrt{2}\eta^{1/2} + 32\eta, \qquad d_{00} \equiv \eta X_2^2\left(K_1 - \frac{X_2^2}{12}\right).$$

Before we can solve (6.12), we need to ensure that the usual Fredholm solvability condition is satisfied. Imposing the orthogonality of the right-hand side on the null space of the differential operator $\mathcal{L}^{\#}$ produces

$$2\eta K_2\int_{-\infty}^{+\infty}A^2(\zeta)\,\mathrm{d}\zeta = d_{13}\int_{-\infty}^{+\infty}B'''(\zeta)A(\zeta)\,\mathrm{d}\zeta + d_{04}\int_{-\infty}^{+\infty}A''''(\zeta)A(\zeta)\,\mathrm{d}\zeta + \int_{-\infty}^{+\infty}d_{00}A^2(\zeta)\,\mathrm{d}\zeta,$$

whence

$$K_2 = \frac{1}{32\omega_0^2}\left(64 + 50\eta - 95\sqrt{2}\eta^{1/2}\right). \tag{6.13}$$

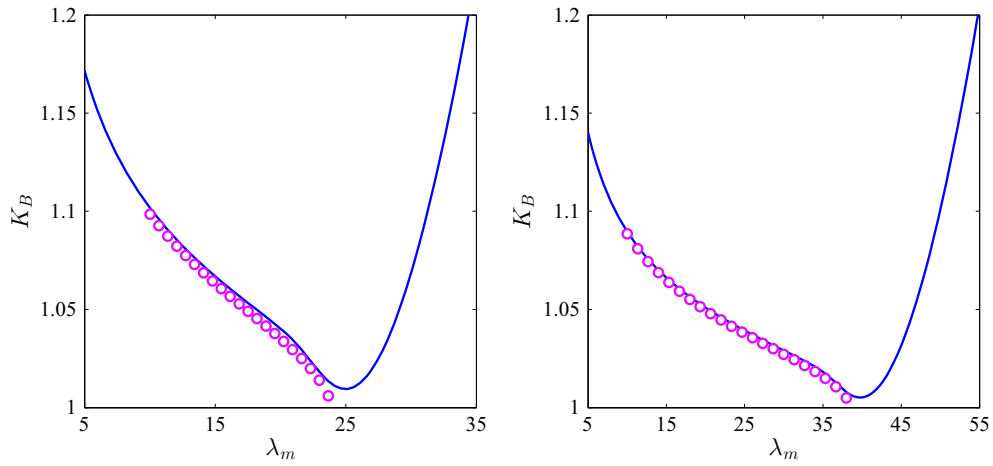

FIG. 10. Left branch comparisons—as per Fig. 9

To compare the three-term asymptotic approximation with full numerical simulations of (2.7)–(2.9), we make the substitution $\eta = \lambda_m^2/\mu$ and finally get

$$K_B = 1 + \sqrt{2}\left(\frac{\sqrt{2}\mu^{1/2} - \lambda_m}{\lambda_m \mu}\right)^{1/2} + \frac{64\mu + 50\lambda_m^2 - 95\sqrt{2}\lambda_m\mu^{1/2}}{32\lambda_m\mu(\sqrt{2}\mu^{1/2} - \lambda_m)} + \ldots. \tag{6.14}$$

Figure 10 illustrates the accuracy of the predictions of (6.14) in relation to direct numerical simulations. In the left window, which corresponds to $R/h = 200$, the relative errors ($R.E.$) range from 0.3% at $\lambda_m \simeq 11$ to 1.6% when $\lambda_m \simeq 24$. For the larger value of $R/h(= 500)$ recorded in the right window of the same figure, the agreement improves; for instance, $R.E. \simeq 0.11\%$ at $\lambda_m \simeq 10$, increasing to 0.14% for $\lambda_m \simeq 25$, while the $R.E.$ is merely 0.3% when $\lambda_m \simeq 37$.

7. A WKB approximation

In the limit $\mu \gg 1$, the original boundary-value problem (2.7)-(2.9) can be also simplified by using the asymptotic strategy proposed by Coman and Haughton [23]. We are going to be primarily interested in the critical case, so we set $\lambda_m^2 = \eta\mu$, for some $\eta = \mathcal{O}(1)$. Letting $H =: \mu\widetilde{H}$ and dividing the first and the second equations in (2.7) by μ and μ^2, respectively, after neglecting the terms $\mu^{-1}(\mathrm{d}^4G/\mathrm{d}\theta^4)$ and $\mu^{-1}(\mathrm{d}^4\widetilde{H}/\mathrm{d}\theta^4)$, we find

$$\begin{cases} -2\eta\dfrac{\mathrm{d}^2G}{\mathrm{d}\theta^2} + \lambda_m^2(\eta - 4K_B\cos\theta)G + \lambda_m^2\widetilde{H} = 0, & \text{(7.1a)} \\ -4\lambda_m^2 G - 2\eta\dfrac{\mathrm{d}^2\widetilde{H}}{\mathrm{d}\theta^2} + \eta\lambda_m^2\widetilde{H} = 0. & \text{(7.1b)} \end{cases}$$

The advantage of this new set of equations lies in the fact that $\widetilde{H}$ can be easily eliminated. Indeed, from (7.1a) we have $\widetilde{H}$ in terms of G and its derivatives, while Eq. (7.1b) allows us to express $d^2\widetilde{H}/d\theta^2$ in a similar way. Differentiating twice (7.1a) and making use of this result leads to the fourth-order differential equation

$$\frac{\mathrm{d}^4G}{\mathrm{d}\theta^4} + 2\lambda_m^2\mathcal{P}(\theta)\frac{\mathrm{d}^2G}{\mathrm{d}\theta^2} + 2\lambda_m^2\mathcal{R}(\theta)\frac{\mathrm{d}G}{\mathrm{d}\theta} + \lambda_m^4\mathcal{Q}(\theta)G = 0, \tag{7.2}$$

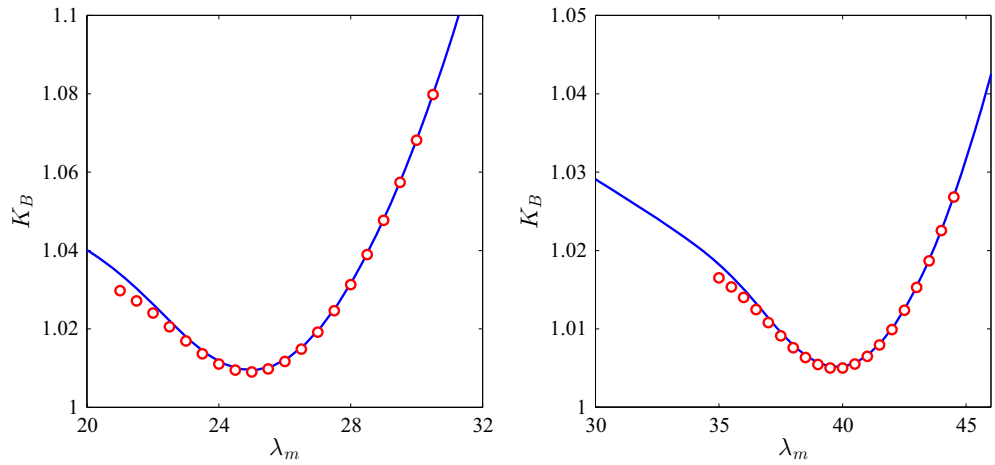

FIG. 11. Comparisons between the approximate equation (7.4) (discrete markers) and direct numerical simulations of the original bifurcation problem (2.7)–(2.9) (*continuous line*) for $\nu = 0.3$; $R/h = 200$ (*left*) and $R/h = 500$ (*right*)

where

$$\mathcal{P}(\theta) := -\frac{1}{2}\left(1 - \frac{2K_B}{\eta}\cos\theta\right), \qquad \mathcal{R}(\theta) := -\frac{2}{\eta}K_B\sin\theta, \tag{7.3a}$$

$$\mathcal{Q}(\theta) := \left[\left(\frac{\eta^2+4}{4\eta^2}\right) - \frac{1}{\eta}\left(1 + \frac{2}{\lambda_m^2}\right)K_B\cos\theta\right]. \tag{7.3b}$$

Since $\lambda_m \gg 1$, Eq. (7.2) is amenable to a WKB treatment that could potentially lead to further approximations for the loading parameter K_B. However, to motivate the analysis that follows it is useful to first gauge the accuracy of (7.2) vis-à-vis the original bifurcation problem. To this end, it will be more convenient to express the approximate equation in a form that features the large parameter (μ) explicitly; straightforward manipulations indicate that such an equation has the form

$$\frac{\mathrm{d}^4G}{\mathrm{d}\theta^4} - (\lambda_m^2 - 2\mu K_B\cos\theta)\frac{\mathrm{d}^2G}{\mathrm{d}\theta^2} - 4\mu K_B\sin\theta\,\frac{\mathrm{d}G}{\mathrm{d}\theta} + \lambda_m^2\left[\frac{\lambda_m^4 + 4\mu^2}{4\lambda_m^2} - \mu\left(1 + \frac{2}{\lambda_m^2}\right)K_B\cos\theta\right]G = 0. \tag{7.4}$$

For a fixed μ—see definition (2.6a), this equation subject to the boundary conditions (2.9) constitutes an eigenvalue problem for $K_B = K_B(\lambda_m)$. We mention in passing that since the number of original boundary conditions on G matches the order of (7.4) no ambiguity arises. In Fig. 11 the 'critical part' of the curve K_B vs. λ_m obtained from (7.4) is compared against the full direct numerical simulations of (2.7)-(2.9). It is clear that even for modest values of R/h the agreement is excellent.

We are going to look for a WKB approximation of (7.2) with an ansatz of the form

$$G(\theta) = \exp\left[\mathrm{i}\lambda_m\Omega(\theta)\right], \qquad \Omega(\theta) := \int_{\bullet}^{\theta}\mathcal{S}_1(\zeta)\,\mathrm{d}\zeta + \lambda_m^{-1}\int_{\bullet}^{\theta}\mathcal{S}_2(\zeta)\,\mathrm{d}\zeta, \tag{7.5}$$

where $\mathrm{i} \equiv \sqrt{-1}$ and the (possibly) complex-valued functions $\mathcal{S}_j$ ($j = 1, 2$) are found as explained below; the lower integration limits in the above integrals are immaterial at this stage (this is indicated by the 'bullet' notation in (7.5b)). We also note in passing that the $\mathcal{O}(\lambda_m^{-2})$ term that enters the expression of $\mathcal{Q}$ in (7.3) can be discarded without impacting the analysis included below.

Substituting (7.5) in (7.2) and then collecting like powers of λ_m show that $S_1 \equiv S_1(\theta)$ satisfies the bi-quadratic

$$t^4 - 2\mathcal{P}(\theta)t^2 + \mathcal{Q}(\theta) = 0, \tag{7.6}$$

whence

$$\mathcal{S}_1^2 = \mathcal{S}_{1j}^2 := \mathcal{P} + (-1)^{j+1}\sqrt{\mathcal{P}^2 - \mathcal{Q}}, \qquad (j = 1, 2). \tag{7.7}$$

To identify the roots of this last equation, it is convenient to introduce the notations

$$\mathcal{S}_{11}^{(\pm)} := \pm\left(\mathcal{P} + \sqrt{\mathcal{P}^2 - \mathcal{Q}}\right)^{1/2} \qquad \text{and} \qquad \mathcal{S}_{12}^{(\pm)} := \pm\left(\mathcal{P} - \sqrt{\mathcal{P}^2 - \mathcal{Q}}\right)^{1/2},$$

and we conclude that $\mathcal{S}_1$ in (7.5) can be taken to be any of these four functions (which is consistent with the fact that our equation is of the fourth order).

Next, the remaining unknown $\mathcal{S}_2 \equiv \mathcal{S}_2(\theta)$ is determined by solving the algebraic equation

$$2\mathrm{i}\mathcal{R}\mathcal{S}_{1j}^{(\pm)} - 4\mathcal{P}\mathcal{S}_{1j}^{(\pm)}\mathcal{S}_2 + 4\mathcal{S}_{1j}^{(\pm)\,3}\mathcal{S}_2 + 2\mathrm{i}\mathcal{P}\mathcal{S}_{1j}^{(\pm)'} - 6\mathrm{i}\mathcal{S}_{1j}^{(\pm)\,2}\mathcal{S}_{1j}^{(\pm)'} = 0, \tag{7.8}$$

where the 'dash' indicates differentiation with respect to θ. Further use of (7.7) and simple manipulations of (7.8) lead to the expression

$$\mathcal{S}_2 = \mathcal{S}_{2j}^{(\pm)} := \frac{\mathrm{i}}{2}\left\{(-1)^{j+1}\frac{\mathcal{P}' - \mathcal{R}}{\sqrt{\mathcal{P}^2 - \mathcal{Q}}} + \frac{\mathrm{d}}{\mathrm{d}\theta}\left[\log(\mathcal{S}_{1j}^{(\pm)}\sqrt{\mathcal{P}^2 - \mathcal{Q}})\right]\right\}, \qquad (j = 1, 2). \tag{7.9}$$

Finally, going back in (7.5) with the functions $\mathcal{S}_j$ $(j = 1, 2)$ found above, we obtain the WKB approximations for a set of four linearly independent solutions of (7.2),

$$G_j^{(\pm)}(\theta) = \frac{1}{\sqrt[4]{\mathcal{S}_{1j}^2(\theta)[\mathcal{P}^2(\theta) - \mathcal{Q}(\theta)]}} \exp\left\{\mathrm{i}\lambda_m \int_\bullet^\theta \mathcal{S}_{1j}^{(\pm)}(\zeta)\,\mathrm{d}\zeta \right.$$
$$\left. - \frac{1}{2}(-1)^{j+1}\int_\bullet^\theta \frac{\mathcal{P}'(\zeta) - \mathcal{R}(\zeta)}{\sqrt{\mathcal{P}^2(\zeta) - \mathcal{Q}(\zeta)}}\,\mathrm{d}\zeta\right\}, \qquad (j = 1, 2). \tag{7.10}$$

These expressions break down when the denominator of the pre-factor multiplying the exponential is zero. In particular, this takes place for those values of $\theta \in [0, \pi]$ for which

$$\mathcal{Q}(\theta) = 0, \quad \text{or} \qquad \cos\theta = \frac{\eta^2 + 4}{4\eta K_B}, \tag{7.11}$$

and

$$\mathcal{P}^2(\theta) - \mathcal{Q}(\theta) = 0, \quad \text{or} \qquad \cos^2\theta = \frac{1}{K_B^2}. \tag{7.12}$$

The solutions of these trigonometric equations define two sets of so-called *turning points* for the differential equation (7.2). The situation we have here is far from straightforward, and a more complete WKB analysis of this equation will be reported elsewhere [33]. In the meantime, we can take advantage of the fact that Steele [32] (see §5.2 in his work) has solved a similar problem (albeit for a somewhat simpler equation) and his analysis can be formally adapted to our case, as explained next.

If we let θ_0 denote the unique root of (7.11) and consider the root $0 < \theta_1 < \pi/2$ of (7.12), it is clear that $\theta_0 < \theta_1$. Steele's quantisation condition [32] expressed in our notation reads $\lambda_m \int_0^{\theta_0} S_{11}^{(+)}(\theta)\,\mathrm{d}\theta = (n - 3/4)\pi$, for $n = 1, 2, \ldots$, with the critical wrinkling load corresponding to $n = 1$. Before we are able to exploit this simple condition, the integrand has to be expressed in terms of θ_0. To this end, we use (7.11) to get K_B as a function of θ_0 and η. If we introduce the function $\mathcal{F}$ defined by

$$\mathcal{F}(\theta; \theta_0, \eta) := \frac{\eta^2 + 4}{4\eta^2}\left[\left(\frac{\cos\theta}{\cos\theta_0} - \frac{2\eta^2}{\eta^2 + 4}\right) + \sqrt{\left(\frac{\cos\theta}{\cos\theta_0}\right)^2 - \frac{16\eta^2}{(\eta^2 + 4)^2}}\right], \tag{7.13}$$

TABLE 1. *Comparison between the asymptotic results (7.15) and full numerical simulations of the bifurcation problem (2.7)–(2.9); here* $\nu = 0.3$

R/h	λ_m^c (asymptotics)	$K_B^{(c)}$ (asymptotics)	λ_m^c (numerical)	$K_B^{(c)}$ (numerical)
300	30.83	1.005600	30.71	1.007204
400	35.66	1.004626	35.61	1.005958
500	39.90	1.004000	39.81	1.005126
700	47.36	1.003193	47.11	1.004100
1000	56.65	1.002518	56.51	1.003228

then the quantisation condition can be cast in the form

$$\int_0^{\theta_0} \sqrt{\mathcal{F}(\theta;\theta_0,\eta)}\,\mathrm{d}\theta = \frac{\pi}{\lambda_m}\left(n-\frac{3}{4}\right), \qquad n=1,2,\ldots. \tag{7.14}$$

To facilitate comparison with the original bifurcation problem (2.7)-(2.9), we still need to replace $\eta = \lambda_m^2/\mu$, but these details are left out in the interest of brevity. For fixed μ and λ_m (i.e. η), Eq. (7.14) can be solved to find the turning point θ_0, so that

$$K_B = \frac{\lambda_m^4 + 4\mu^2}{4\lambda_m^2\mu\cos\theta_0}. \tag{7.15}$$

By minimising this expression with respect to λ_m, we can then obtain a WKB approximation for the critical wrinkling load. In Table 1, we exemplify the quality of these predictions by comparison of the critical values λ_m^c and $K_B^{(c)}$ with some direct numerical computations of the full system over a range of values of the ratio $3\times 10^2 \le R/h \le 10^3$. It is clear that agreement is excellent in all of the cases included in our table.

8. Concluding remarks

The onset of partial wrinkling in a thin elastic cylinder subjected to in-plane bending has been revisited from the point of view of multiple-scale asymptotics. Our main interest has been in understanding the multi-scale structure of the neutral stability curves obtained previously by Seide and Weingarten [9]. These curves have a parabola-like appearance, with the vertex corresponding to the energy-minimum configuration of the wrinkled cylinder. By a suitable introduction of a large parameter $\mu \propto R/h \gg 1$, we have showed that the left branches of these curves involve the interplay between two distinct spatial scales, $X_1 = \mathcal{O}(\mu^{1/2})$ and $X_2 = \mathcal{O}(\mu^{1/4})$, respectively. As we approach the vertex, the fast scale weakens its effect, while close to the vertex the slow scale changes to $X_3 = \mathcal{O}(\mu^{1/3})$. Furthermore, to the right of the vertex the behaviour changes once again, with the system now evolving on an $\mathcal{O}(\mu^{1/4})$ scale. This overall picture has been augmented by an expedient solution based on the classical WKB method. Although this route has the advantage of producing a leading-order approximation with minimum effort, it is not immediately clear how one might pursue higher-order terms systematically.

Comparisons between the asymptotic predictions obtained and full numerical simulation of the bifurcation equations have revealed unusually good agreement, even for modest values of the ratio R/h. Of course, this is a direct consequence of the fact that the differential operators that appear in the bifurcation system have constant coefficients and the only variable term occurs in the expression of $\mathcal{L}_{11}$ (cf. (2.8)). Nevertheless, the asymptotic methods used in this paper are not limited in any way by the complexity of the coefficients of the differential equations in question. We remark in passing that the method of multiple scales can be used to investigate the post-buckling behaviour of the cylindrical shell and its imperfection sensitivity as was done, for instance, in [27,34] for some simpler problems.

The membrane pre-buckling state adopted in [9] (and in our Sect. 2) does impose some limitations, not only because of its intrinsic linearity but also due to the fact that its expression is length independent. The analysis presented in this work is expected to be valid for cylinders with $L/R \simeq \mathcal{O}(1)$; longer cylinders would require the inclusion of nonlinear effects and taking into account the progressive ovalisation of the cross section within the pre-buckling range. This aspect has also been recently completed by the author [35].

References

[1] Yamaki, N.: Elastic Stability of Circular Cylindrical Shells. North-Holland, Amsterdam (1984)
[2] Kyriakides, S., Corona, E.: Mechanics of Offshore Pipelines 1: Buckling and Collapse. Elsevier Science, Oxford (2007)
[3] Axelrad, E.L.: Theory of Flexible Shells. North-Holland, Amsterdam (1987)
[4] Brazier, L.G.: On the flexure of thin cylindrical shells and other thin sections. Proc. Roy. Soc. A **116**, 104–114 (1927)
[5] Singer, J., Arbocz, J., Weller, T.: Buckling Experiments: Experimental Methods in Buckling of Thin-Walled Structures, vol. 2. Wiley, New York (2002)
[6] Kyriakides, S., Ju, G.T.: Bifurcation and localization instabilities in cylindrical shells under bending, part 1: experiments. Int. J. Solids Struct. **29**, 1117–1142 (1992)
[7] Emmerling, F.A.: Nonlinear bending of curved tubes. In: Axelrad, E.L., Emerling, F.A. (eds.) Flexible Shells: Theory and Applications, pp. 44–63. Springer, Berlin (1984)
[8] Flügge, W.: Die Stabilitat der Kreiszylinderschale. Ing. Archiv. **3**, 463–506 (1932)
[9] Seide, P., Weingarten, V.I.: On the buckling of circular cylindrical shells under pure bending. ASME J. Appl. Mech. **28**, 112–116 (1961)
[10] Troger, H., Steindl, A.: Nonlinear Stability and Bifurcation Theory. Springer, Wien (1991)
[11] Gould, P.L.: Analysis of Plates and Shells. Prentice Hall, Upper Saddle River (1999)
[12] Axelrad, E.L.: Refinement of the upper critical loading of pipe bending, taking account of the geometrical nonlinearity (in Russian). Izvestiia, AN, USSR, OTN, Mekhanika i Mashinostroenie **4**, 123–139 (1965)
[13] Axelrad, E.L.: On local buckling of thin shells. Int. J. Non Linear Mech. **20**, 249–259 (1985)
[14] Reissner, E., Weinitschke, H.J.: Finite pure bending of circular cylindrical tubes. Q. Appl. Math. **20**, 305–319 (1963)
[15] Fabian, O.: Collapse of cylindrical elastic tubes under combined bending, pressure and axial loads. Int. J. Solids Struct. **13**, 1257–1270 (1977)
[16] Stephens, W.B., Starnes, J.H., Almroth, Bo O.: Collapse of long cylindrical shells under combined bending and pressure loads. AIAA J. **13**, 20–25 (1975)
[17] Corona, E., Vaze, S.P.: Buckling of elastic-plastic tubes under bending. Int. J. Mech. Sci. **38**, 753–775 (1996)
[18] Nayfeh, A.H., Mook, D.T.: Nonlinear Oscillations. Wiley, New York (1979)
[19] Tam, K.K.: On the asymptotic solution of the Orr-Sommerfeld equation by the method of multiple-scales. J. Fluid Mech. **34**, 145–158 (1968)
[20] Long, L.N.: Uniformly-valid asymptotic solutions to the Orr-Sommerfeld equation using multiple scales. J. Eng. Math. **21**, 167–178 (1987)
[21] Wollkind, D.J.: Singular perturbation techniques: a comparison of the method of matched asymptotic expansions with that of multiple scales. SIAM Rev. **19**, 502–516 (1977)
[22] Bouthier, M.: Comparison of the matched asymptotic expansions method and the two-variable technique. Q. Appl. Math. **41**, 407–422 (1984)
[23] Coman, C.D., Haughton, D.M.: Localized wrinkling instabilities in radially stretched annular thin films. Acta Mech. **185**, 179–200 (2006)
[24] Coman, C.D.: Remarks on elastic buckling for sectorial plates. Int. J. Eng. Sci. **47**, 1002–1013 (2009)
[25] Coman, C.D.: Some applications of the WKB method to the wrinkling of bi-annular plates in tension. Acta Mech. **224**, 399–423 (2013)
[26] Tovstik, P.E., Smirnov, A.L.: Asymptotic Methods in the Buckling of Elastic Shells. World Scientific Publishing, Singapore (2001)
[27] Coman, C.D.: Localized elastic buckling: non-linearities versus inhomogeneities. IMA J. Appl. Math. **75**, 461–474 (2010)
[28] Batdorf, S.B.: A simplified method of elastic-stability analysis for thin cylindrical shells. Report No. 874, Langley Memorial Aeronautical Laboratory, Langley Field, Va., pp. 25 (1947)
[29] Libai, A., Durban, D.: Buckling of cylindrical shells subjected to non-uniform axial loads. ASME J. Appl. Mech. **44**, 714–720 (1977)
[30] Lebedev, N.N.: Special Functions and Their Applications. Dover Publications Inc., New York (1972)
[31] Coman, C.D.: On interactive buckling in a sandwich structure. Z. Angew. Math. Phys. **61**, 565–577 (2010)

[32] Steele, C.R.: Application of the WKB method in solid mechanics. In: Nemat-Nasser, S. (ed.) Mechanics Today, vol. 3, pp. 243–295. Pergamon Press, New York (1976)
[33] Coman, C.D.: Uniform asymptotic approximations for a fourth-order differential equation with coalescing turning points. (in preparation)
[34] Amazigo, J.C., Budiansky, B., Carrier, G.F.: Asymptotic analyses of the buckling of imperfect columns on nonlinear elastic foundations. Int. J. Solids Struct. **6**, 1341–1356 (1970)
[35] Coman, C.D.: Bifurcation instabilities in finite bending of circular cylindrical shells. Int. J. Eng. Sci. **119**, 249–264 (2017). doi:10.1016/j.ijengsci.2017.06.022

Ciprian D. Coman
West Molesey, Surrey KT8 1NY
UK
e-mail: cdc3p@yahoo.com

(Received: March 25, 2017)